

# Transmission of a microwave cavity coupled to localized Shiba states

Razvan Chirla,<sup>1</sup> Andrei Manolescu,<sup>2</sup> and Cătălin Pașcu Moca<sup>3,1</sup>

<sup>1</sup>*Department of Physics, University of Oradea, 410087, Oradea, Romania*

<sup>2</sup>*School of Science and Engineering, Reykjavik University, Menntavegur 1, IS-101 Reykjavik, Iceland*

<sup>3</sup>*BME-MTA Exotic Quantum Phase Group, Institute of Physics,  
Budapest University of Technology and Economics, H-1521 Budapest, Hungary*

(Dated: July 7, 2021)

We consider a strongly correlated quantum dot, tunnel coupled to two superconducting leads and capacitively coupled to a single mode microwave cavity. When the superconducting gap is the largest energy scale, multiple Shiba states are formed inside the gap. The competition of these states for the ground state signals a quantum phase transition. We demonstrate that photonic measurements can be used to probe such localized Shiba states. Moreover, the quantum phase transition can be pinpointed exactly from the sudden change in the transmission signal. Calculations were performed using the numerical renormalization group approach.

PACS numbers: 42.50.-p, 72.10.Fk, 72.15.Qm, 73.63.Kv

## I. INTRODUCTION

Quantum circuits combining elements of atomic physics, quantum optics, mesoscopic condensed matter physics and topological materials, could pave the way to the realization of fault-tolerant quantum computers [1]. In such a hybrid circuit, a microwave coplanar waveguide resonator can act as a data bus between components of the setup. In particular, it has been shown experimentally that an artificial atom, such as a superconducting qubit [2], a quantum dot (QD) [3–6], an Andreev dot [7], or a double quantum dot [8–10] coupled to a photon cavity, produces a measurable effect on the amplitude and phase of the transmitted electromagnetic field, as well as a shift and broadening of the resonant frequency of the cavity. The state-dependent frequency pull by the artificial atom can be used to entangle the state of the atom with that of the photons that pass through the resonator [11, 12]. By choosing an appropriate driving frequency, high efficiency quantum non-demolition readout measurements of the state of the atom can be performed, or alternatively, the state of the atom can be coherently controlled [7].

So far, the coupling between mesoscopic systems and microwave resonators has been studied by either neglecting the repulsive interaction between electrons [13–16], by modeling the device as a two-level system [10], or employing various other approximations [17–19].

In the present work we investigate the response of a hybrid QD-resonator device by computing the phase and the amplitude of the transmitted signal as function of the incoming microwave frequency. The system is displayed in Fig. 1 and consists of a quantum dot setup coupled capacitively to a microwave resonator. The dot is tunnel coupled to two superconducting leads. Such a system presents localized states inside the superconducting gap – also known as Shiba states [20]. These are resonant states with a given parity [21] (in our description they are either singlet or double states in the spin sector). They are competing to form the ground state, implicitly

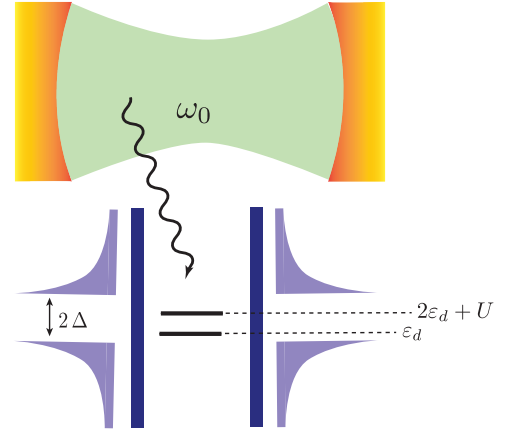


FIG. 1. (Color online) Sketch with the setup. An interacting quantum dot with on-site energy  $\varepsilon_d$  and Coulomb repulsion  $U$ , is coupled to two superconducting leads. The dot is capacitively coupled to a microwave cavity. The cavity is assumed to support a single mode with frequency  $\omega_0$ . The superconducting gap,  $\Delta$  is the largest energy scale.

driving the system through a quantum phase transition (QPT). On one side of the transition, when the ground state is a doublet, the photonic cavity is insensitive to the presence of the electronic system and the transmission is unaffected, while on the other side of the transition, when the ground state is a singlet, the Shiba states are expected to be responsive when probed by the cavity [7]. We indeed find that, by attaching the cavity to a pair of external transmission lines, both the amplitude and the phase difference between the outgoing and incoming fields carry the fingerprint of the interaction between the cavity and the electronic system, and furthermore one obtains direct information on the energies of the Shiba states. Moreover, if the system is driven across the QPT by tuning a control parameter, such as  $\varepsilon_d$  or  $\Gamma$ , we expect a sudden change in the transmitted signal as some of the

transitions between the Shiba states become active. In this way, the presence and the position of the quantum critical point (QCP) can be accurately detected.

## II. SYSTEM AT EQUILIBRIUM

### A. Model Hamiltonian

Our system consists of a quantum dot that is coupled to two superconducting leads at equilibrium. The dot is also capacitively coupled to a microwave cavity (see Fig. 1). The setup is described in terms of the Anderson model, which by now emerges as a standard approach to study electron transport in such nanodevices. In this framework, the system Hamiltonian,  $H_{\text{sys}}$ , consists of several terms. The dot itself can be modeled by a spinful interacting level of energy  $\varepsilon_d$ , with a Coulomb interaction strength  $U$ . The dot Hamiltonian can be written in terms of the occupation  $\hat{n} = \hat{n}_\uparrow + \hat{n}_\downarrow$  as

$$H_{\text{dot}} = \varepsilon_d \hat{n} + U \hat{n}_\uparrow \hat{n}_\downarrow, \quad (1)$$

where  $\hat{n}_\sigma = d_\sigma^\dagger d_\sigma$  ( $\sigma = \{\uparrow, \downarrow\}$ ), and  $d_\sigma^\dagger$  are the creation operators on the QD. The localized orbital hybridizes with the states in the two superconducting leads via the tunneling Hamiltonian

$$H_{\text{tun}} = \sum_{\alpha=\{L,R\}} \sum_{\sigma} (V_\alpha d_\sigma^\dagger \psi_{\alpha\sigma}(0) + \text{H.C.}). \quad (2)$$

We assume a left-right symmetry,  $V_\alpha = V$ , where  $\alpha = \{L, R\}$ , and a tunneling rate  $\Gamma = 2\pi \varrho_0 V^2$ . Here  $\varrho_0 = 1/2D$  is the constant density of states of a conduction band. In what follows,  $D = 1$  will serve as the energy unit.  $\psi_{\alpha\sigma}(\mathbf{R})$  is the field operator for the conduction electrons,  $\psi_{\alpha\sigma}(\mathbf{R}) = \int \frac{d\mathbf{k}}{(2\pi)^3} c_{\alpha\mathbf{k}\sigma} e^{-i\mathbf{k}\mathbf{R}}$ , and  $c_{\alpha\mathbf{k}\sigma}$  are the annihilation operators for the conduction band electrons in lead  $\alpha$ , with momentum  $\mathbf{k}$  and spin  $\sigma$ . They satisfy the anticommutation relations:  $\{c_{\alpha\mathbf{k}\sigma}, c_{\alpha'\mathbf{k}'\sigma'}^\dagger\} = (2\pi)^3 \delta(\mathbf{k} - \mathbf{k}') \delta_{\sigma\sigma'}$ . The dot is also capacitively coupled to the cavity

$$H_{\text{int}} = g \hat{n} (a + a^\dagger), \quad (3)$$

with  $g$  the strength of the light-matter coupling, and  $a^\dagger$  a bosonic operator describing the creation of a photon in the cavity. In our approach we assume that the resonator supports a single monochromatic mode  $\omega_0$ , so that the cavity Hamiltonian reduces simply to

$$H_{\text{cav}} = \hbar \omega_0 a^\dagger a. \quad (4)$$

Most of the theoretical approaches neglect the back-action from the cavity on the electronic states, and restore a finite coupling when investigating the dynamics of the photons only. This is a well suited approximation for the tunneling junctions [22] or QDs [12, 14] coupled to normal leads as long as the inter-level energy spacing of

the electronic system  $\delta_l \ll \hbar \omega_0$ , otherwise the decoupling of the photons from the QD is no longer possible, and the electronic transport is affected [18, 19]. This condition is not satisfied in our setup, as the energy of the excited Shiba states inside the superconducting gap,  $E_S \sim \hbar \omega_0$ , so decoupling the photons from the QD is not possible. The resonant coupling between the cavity and the QD is evident from the avoided level crossing between the gap states (see Fig. 2(b) for details.)

Finally, the metallic leads that couple to the dot are considered as BCS superconductors and are described by the Hamiltonian

$$H_{\text{leads}} = \sum_{\alpha=\{L,R\}} \int \frac{d\mathbf{k}}{(2\pi)^3} \sum_{\sigma} \xi_{\alpha\mathbf{k}\sigma} c_{\alpha\mathbf{k}\sigma}^\dagger c_{\alpha\mathbf{k}\sigma} + (\Delta_\alpha c_{\alpha\mathbf{k}\uparrow}^\dagger c_{\alpha-\mathbf{k}\downarrow}^\dagger + \text{H.C.}). \quad (5)$$

In Eq. (5),  $\Delta_\alpha = |\Delta| e^{-i\varphi_\alpha}$  stands for the superconducting gap in lead  $\alpha$ . For simplicity we use  $\varphi_\alpha = 0$  in what follows. We first study the ground state, excitation spectrum and the spectral properties of the system Hamiltonian

$$H_{\text{sys}} = H_{\text{dot}} + H_{\text{cav}} + H_{\text{tun}} + H_{\text{int}} + H_{\text{leads}}, \quad (6)$$

by treating all the interactions in the setup on equal footing. We call this an equilibrium configuration in the sense that the cavity is not connected to the external transmission lines, but only to the quantum dot. As a method we use the numerical renormalization group (NRG) [23, 24], in a manner similar to how it was done previously for the Anderson-Holstein model [25, 26]. Details of the NRG calculations are provided in Appendix A. In our numerical calculations we consider only the particle-hole symmetrical situation, i.e.  $\varepsilon_d = -U/2$ . Although we are always at the particle-hole symmetrical point, we shall not perform the calculations in the Kondo limit [27] (corresponding to  $-\varepsilon_d = U/2 \rightarrow \infty$ ), but allow for large quantum charge fluctuations. In our calculations, the charging energy of the dot is always smaller than the superconducting gap, i.e.  $\Delta > \{U, |\varepsilon_d|\}$ . This is a required condition for the second singlet-like excited Shiba state (labeled  $S_+$  in Fig. 2 (a)) to survive inside the gap. In this way, the superconducting gap supports two bound states of the same parity, which allows photonic transitions between them [7].

For a better understanding of the whole picture we shall also discuss shortly the physics of the electronic part of the system in the absence of the photons. It corresponds to the Hamiltonian

$$H_{\text{el}} = H_{\text{dot}} + H_{\text{tun}} + H_{\text{leads}}. \quad (7)$$

Although the NRG is a powerful and exact method, the results are not always intuitive enough, and for that, we shall supplement our NRG results, where possible, with analytical descriptions.

## B. Shiba states

### 1. Shiba states in the absence of photons

So far, the Hamiltonian  $H_{\text{el}}$  given in Eq. (7) which does not include the coupling to the resonant cavity, has been studied extensively in the literature [20, 28, 29]. In the limit when charge fluctuations are frozen,  $U \rightarrow \infty$ , a pair of states develops in the gap: a singlet-like state (labeled  $S_-$  in Fig. 2) and a doublet  $D_\sigma$ . Depending on the setup parameters, each of these states can be the ground state. Consequently, the system develops a quantum phase transition. This transition can be understood as the competition between the superconducting correlations and the Kondo screening, and takes place when  $\Delta \sim T_K$ . Here  $T_K$  is the Kondo temperature characterizing  $H_{\text{el}}$  when the external leads are in the normal state. On one side of the transition, when  $\Delta > T_K$ , the ground state is the doublet  $D_\sigma$ , as the local moment remains unscreened, while on the other side,  $\Delta < T_K$ , the Kondo screening wins and the ground state becomes the many-body Kondo singlet  $S_-$ .

If charge fluctuations are allowed, and if  $U < \Delta$ , a second singlet state  $S_+$  develops inside the gap. In the non-interacting limit, when  $U \rightarrow 0$ , its energy is exactly  $E_{S_+} = 2E_{D_\sigma}$  [30]. Increasing  $U$  sufficiently, its energy starts to shift to larger values, and when  $U \sim \Delta$ , it merges with the continuum.

As we are interested in the bound states inside the gap, it is natural to consider the  $\Delta \rightarrow \infty$  limit. It was previously shown [31] that the QPT transition can be nicely captured in this limit, and that an effective model can be constructed by integrating out the leads:

$$H_{\text{el}}^{(\Delta \rightarrow \infty)} = \sum_{\sigma} \xi_d d_{\sigma}^{\dagger} d_{\sigma} - \Gamma \left( d_{\uparrow}^{\dagger} d_{\downarrow}^{\dagger} + \text{h.c.} \right) + \frac{U}{2} (\hat{n} - 1)^2, \quad (8)$$

where  $\xi_d = \varepsilon_d + U/2$ . The Hamiltonian in Eq. (8) can be diagonalized in a local basis as

$$H_{\text{el}}^{(\Delta \rightarrow \infty)} = \sum_{\gamma=\pm, \sigma} E_{\gamma} |\gamma\rangle \langle \gamma|. \quad (9)$$

With the notations  $u = (1 + \xi_d/2E_d)/2$  and  $v = (1 - \xi_d/2E_d)/2$ , where  $E_d = \sqrt{\xi_d^2 + \Gamma^2}$ , the eigenstates can be grouped into a pair of singlets  $|\pm\rangle$ :  $|+\rangle = (u d_{\uparrow}^{\dagger} d_{\downarrow}^{\dagger} + v)|0\rangle$ ,  $|-\rangle = (-v^* d_{\uparrow}^{\dagger} d_{\downarrow}^{\dagger} + u)|0\rangle$ , and a doublet  $|\sigma\rangle = d_{\sigma}^{\dagger}|0\rangle$ . The corresponding energies are  $E_{\pm} = \xi_d + U/2 \pm \sqrt{\xi_d^2 + \Gamma^2}$  and  $E_{\sigma} = \xi_d$ . Since  $E_- < E_+$ , the QPT is recovered when the singlet  $|-\rangle$  and the doublet state  $|\sigma\rangle$  are degenerate in energy:  $E_- = E_{\sigma}$ . Since  $\Delta \rightarrow \infty$ , all these states in Eq. (9) are actually resonant levels that live inside the gap and are the so-called Shiba states [20]. In this limit, there is a one to one correspondence with the states obtained in the NRG:  $|\pm\rangle \leftrightarrow S_{\pm}$  and  $|\sigma\rangle \leftrightarrow D_{\sigma}$ .

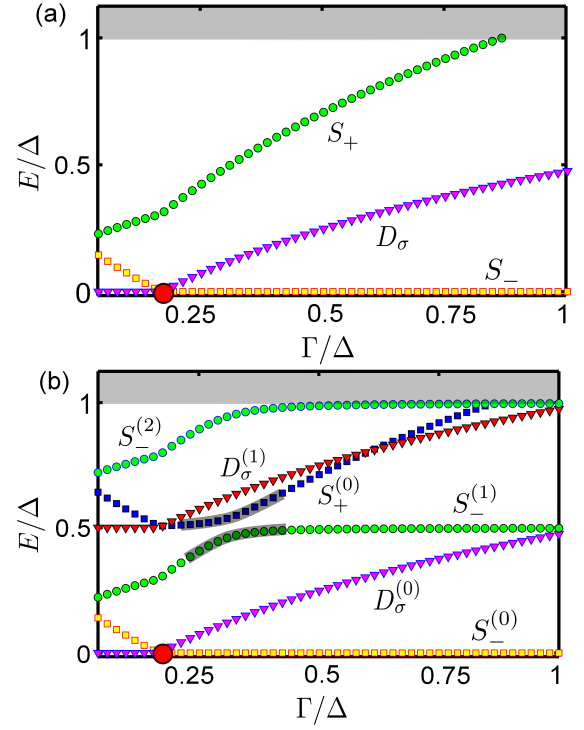


FIG. 2. (Color online) (a) Shiba states inside the gap in the absence of photons. The QCP is marked by the red dot. (b) Shiba states in the presence of the photons. The other parameters are fixed to:  $\omega_0/\Delta = 0.5$ ,  $g/\Delta = 0.05$  and  $U/\Delta = 0.4$ . For this set of parameter the quantum critical point corresponds to  $x_{\text{QCP}} = (\Gamma/\Delta)_{\text{QCP}} \simeq 0.17$ . The shaded lines emphasize the avoided level crossing. The shaded area above  $E = \Delta$  represents the continuum.

### 2. Shiba states and the Jaynes-Cummings Hamiltonian

In the presence of a cavity, these states start to hybridize with the photons. Since the operator  $\hat{n}$  entering Eq. (3) is charge conserving,  $H_{\text{int}}$  couples only states with the same parity. Moreover, in the absence of the external field, the doublet states are always degenerate in energy, so there is no dipole matrix element between them, and they remain decoupled from the photonic field. In that regard, the following discussion is suitable for the singlet side of the QPT, where the singlet  $|-\rangle$  is the ground state and the singlet  $|+\rangle$  is the excited state. Computing the dipole matrix element  $\langle + | \hat{n} | - \rangle = -2uv$ , and introducing the regular notations  $\sigma^+ = |+\rangle \langle -|$ ,  $\sigma^- = (\sigma^+)^{\dagger}$ , and using the rotating wave approximation, the Hamiltonian  $H_{\text{sys}}$  in Eq. (6) can be rewritten simply as a Jaynes-Cummings Hamiltonian [32] in the singlet sector plus a non-interacting part in the doublet sector

$$H_{\text{sys}}^{(\Delta \rightarrow \infty)} = \frac{1}{2} \hbar \omega_A \sigma^z + \hbar \omega_0 a^{\dagger} a - \hbar \tilde{g} (a \sigma^+ + \sigma^- a^{\dagger}) + \sum_{\sigma=\{\uparrow, \downarrow\}} E_{\sigma} |\sigma\rangle \langle \sigma|, \quad (10)$$

where we have introduced the notations  $\hbar\omega_A = 2E_d$  and  $\hbar\tilde{g} = g(\Gamma/E_d)$ . This two-level system coupled to a photonic field has been studied thoroughly by now [33], so we won't discuss it further here.

### 3. Energy spectrum

In this section we discuss in more detail the NRG results for the energy spectrum in the limit when  $\Delta$  is the largest energy scale in the problem, i.e.  $\Delta \gg \{|\varepsilon_d|, U, \Gamma, \hbar\omega_0\}$ . We shall ignore the continuum  $E > \Delta$  and discuss only the localized states.

We start by presenting in Fig. 2(a) the evolution of the Shiba states for  $H_{\text{el}}$  as function of  $x = \Gamma/\Delta$  in the absence of the photons. For  $x \leq x_{\text{QCP}}$ , the ground state consists of a BCS superconductor plus a free local moment (doublet ground state  $D_\sigma$ ), while in the other limit, when  $x > x_{\text{QCP}}$ , the local spin screened by the conduction electrons forms a many-body singlet ground state ( $S_-$ ). The other singlet state  $S_+$  is always higher in energy and never competes for the ground state. The QCP corresponds to the degeneracy in energy of the levels  $S_-$  and  $D_\sigma$  (marked by a red dot in Fig. 2).

In Fig. 2(b) we show the same Shiba states in the presence of the photonic field. The spectrum was obtained by solving the Hamiltonian (6) exactly, with 5 photons in the system. We have checked that by adding extra photons, the spectrum inside the gap remains the same, and only higher energy states in the continuum are affected. Throughout our calculations, the photon energy is fixed to  $\omega_0 = \Delta/2$ . First of all, except for a small Stark shift towards the doublet sector as  $g$  is further increased, the photons have a negligible impact on the position of the QCP. Moreover, as the doublet state does not hybridize with the photonic states (there is no dipole matrix element), its energy remain unaffected, so that we can only see the formation of equally separated energy states in this channel (ladder states, labeled as  $D_\sigma^{(0)}, D_\sigma^{(1)}, \dots$ ). On the other hand, the photonic states hybridize with electronic ones in the singlet channel, and this is signaled by the formation of the avoided level crossing when  $\omega_0 \simeq E_{S_+}$ . In Fig. 2(b) this is highlighted by the shaded lines at  $x \simeq 0.3$ . The labeling of the lines emphasizes both to which electronic states they belong, and the number of photons used to build the states in the singlet sector, far away from the resonance.

Although in Fig. 2(b) we present the situation when the position of the avoided level crossing is on the singlet side of the QPT, its position as function of  $x$  can be tuned to the other side of the QPT by simply tuning some control parameter, such as  $\omega_0$ . Notably, in Ref. [7], this resonant coupling has been measured recently by using a circuit quantum electrodynamic setup coupled to an Andreev qubit.

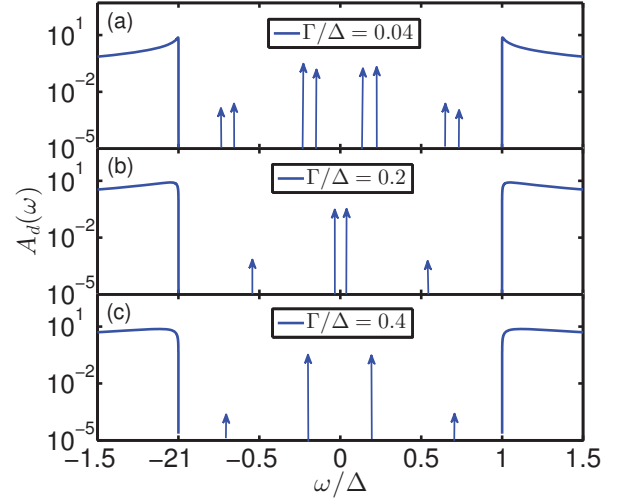


FIG. 3. (Color online) Spectral function for the on-site creation operator  $d_\sigma^\dagger$  at  $T=0$ . The weights and positions for the transitions between the ground state and the excited Shiba states are indicated by vertical arrows. They correspond to the transitions between:  $D_\sigma^0 \leftrightarrow \{S_-^{(0)}, S_+^{(0)}, S_-^{(1)}, S_-^{(2)}\}$  for  $\Gamma/\Delta = 0.04$  when the ground state is  $D_\sigma$ , and to  $S_-^{(0)} \leftrightarrow \{D_\sigma^{(0)}, D_\sigma^{(1)}\}$  when  $\Gamma/\Delta = \{0.2, 0.4\}$ , when the ground state is  $S_-$ .

### C. Electronic spectral functions

Here we discuss the results for the spectral function  $A_d(\omega)$  of the operator  $d_\sigma^\dagger$ :

$$A_d(\omega) = -\frac{1}{\pi} \text{Im } G_d(\omega), \quad (11)$$

with  $G_d(\omega)$  being the Fourier transform of the electronic Green's function:  $G_d(t) = -i\theta(t) \langle \{d_\sigma(t), d_\sigma^\dagger(0)\} \rangle$ . Since  $d_\sigma^\dagger$  is a charge  $q = 1$  operator, only the transitions between the ground state and the excited Shiba states, having different parity, are visible in the spectral density  $A_d(\omega)$ . For  $x < x_{\text{QCP}}$  (panel (a) in Fig. 3) the ground state is the doublet  $D_\sigma$ . In this case, the transitions  $D_\sigma^{(0)} \rightarrow S_\pm^{(n)}, n = 0, 1, \dots$  are active. For our set of parameters, there are four such singlet excited states inside the gap, implying four visible particle-like resonances for  $\omega > 0$ . The associated pairs are the hole-like transitions at negative frequencies. In the singlet phase, the number of resonances reduces to half (see panels (b) and (c) in Fig. 3), as the transitions  $S_-^{(0)} \rightarrow S_\pm^{(n)}$  become forbidden by symmetry.

The observation of the Shiba states can be achieved by measuring the cavity transmission or reflection [7]. In that regard, the change in the output signal gives information about the electronic susceptibility. In Fig. 4 we display the spectral function for the dot occupation operator,  $\hat{n} = \hat{n}_\uparrow + \hat{n}_\downarrow$ , that corresponds to the dissipative part of the electronic susceptibility. The transitions between the states with the same parity are now visible. This is the reason why in the singlet region, when



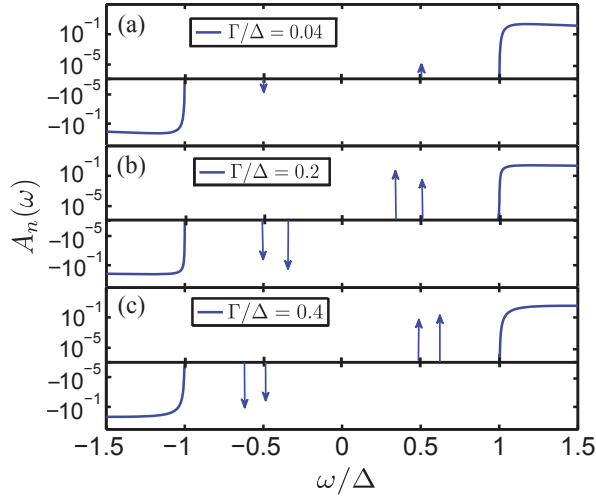


FIG. 4. (Color online) Bosonic spectral function for the occupation number operator of the dot,  $\hat{n}$  at  $T=0$ . The transitions inside the gap are between the ground state and excited states with the same parity.

$x > x_{\text{QCP}}$ , two transitions are visible, corresponding to  $S_-^{(0)} \rightarrow \{S_-^{(1)}, S_+^{(0)}\}$ . Therefore, for our specific setup, this quantity gives direct information on the existence of and transitions between various Shiba states. This will be discussed in more detail in Sec. III.

### III. MICROWAVE PROBED CAVITY

So far we have discussed the system at equilibrium, but our main goal is to probe the Shiba states through photon transport. For that, the resonator is coupled capacitively to two external transmission lines that transmit the input and output microwave signal. The total Hamiltonian takes the form

$$H = H_{\text{sys}} + \sum_{\beta=\{L,R\}} \sum_{\mathbf{q}} \left[ \omega_{\mathbf{q}} b_{\beta\mathbf{q}}^\dagger b_{\beta\mathbf{q}} + \lambda_{\mathbf{q}} (b_{\beta\mathbf{q}}^\dagger + b_{\beta\mathbf{q}}) (a + a^\dagger) \right]. \quad (12)$$

Here  $b_{\beta\mathbf{q}}^\dagger$  is the creation operator of a photonic mode  $\mathbf{q}$  in the transmission line  $\beta = \{L, R\}$  with photon energy  $\omega_{\mathbf{q}}$ . Inside the resonator the dissipation of energy occurs through two channels:

(i) capacitive coupling to the external photon bath with strength  $\lambda_{\mathbf{q}}$ . In this channel the photons leak out of the cavity at a rate [17]

$$\begin{aligned} \mathcal{J}(\omega) &= \pi \sum_{\mathbf{q}} \lambda_{\mathbf{q}}^2 \delta(\omega - \omega_{\mathbf{q}}) \\ &\simeq 2\pi \alpha \omega e^{-\omega/\omega_c}, \end{aligned} \quad (13)$$

with  $\omega_c$  some energy cutoff. In most of the cases, as the driving frequency is close to the resonant frequency of the cavity,  $\omega \simeq \omega_0$ , the escape rate of the cavity  $\kappa$  is

approximately constant and given by  $\kappa = 2\pi \alpha \omega_0$ , where  $\alpha$  is a dimensionless constant.

(ii) The electron-photon interaction is the second channel of decay [8, 14]. Besides the dissipative effects [34], it can also cause a shift of the resonance frequency. It was observed that the quantum shot noise of the coherent conductor under the ac-bias can squeeze the photonic field [35]. Recent theoretical studies [14] indicate that in the limit when the charge susceptibility is small, i.e.  $|\Pi(\omega)| \ll \kappa$ , the ratio  $\Pi'(\omega)/\kappa$  approximates the phase shift and  $\Pi''(\omega)/\kappa$  corresponds to the cavity peak broadening, where the primed and double-primed quantities are the real and imaginary parts of the charge susceptibility.

#### A. Green's function for the photons

In this section we present the results for the spectral function  $A_{a+a^\dagger}(\omega)$  of the photonic operator  $a + a^\dagger$ . This quantity is needed for the evaluation of the microwave transmission across the cavity. The retarded Green's function for the photons is defined as

$$\mathcal{D}^R(t) = -i\Theta(t) \langle [a(t) + a^\dagger(t), a(0) + a^\dagger(0)] \rangle. \quad (14)$$

The spectral function is obtained in terms of its Fourier transform  $\mathcal{D}^R(\omega)$  as

$$A_{a+a^\dagger}(\omega) = -\frac{1}{\pi} \text{Im} \mathcal{D}^R(\omega). \quad (15)$$

In the absence of any sources of dissipation, the non-interacting correlator is

$$\mathcal{D}_0^R(\omega) = \frac{2\omega_0}{\omega^2 - \omega_0^2 + i0^+}. \quad (16)$$

There are several ways to compute the spectral function, either directly from the NRG, or by including the self-energy correction, as was originally proposed for the Anderson model in Ref. [36], and later applied to the Anderson-Holstein model [26]. We have used the latter approach, as the sum rule is better satisfied. The method consists in using the equation of motion for some correlators in order to evaluate the photonic self-energy (see Appendix B for details), and then the use of Dyson equation to compute the full Green's function

$$\mathcal{D}^R(\omega)^{-1} = \mathcal{D}_0^R(\omega)^{-1} - \Sigma_{\text{el}}(\omega) - \Sigma_{\text{ph}}(\omega). \quad (17)$$

Here,  $\Sigma_{\text{ph}}(\omega)$  incorporates dissipation effects from the photon system only, coming from the coupling of the cavity to the external modes,  $\Sigma_{\text{ph}}(\omega) = -i\kappa/2$ . In Eq. (17), the part of the self-energy coming from the light-matter interaction is obtained as

$$\Sigma_{\text{el}}(\omega) = g \frac{\mathcal{F}^R(\omega)}{\mathcal{D}^R(\omega)}, \quad (18)$$

where  $\mathcal{F}(\omega)$  is the Fourier transform of the bosonic Green's function:  $\mathcal{F}^R(t) = -i\Theta(t) \langle [\hat{n}(t), a(0) + a^\dagger(0)] \rangle$ .

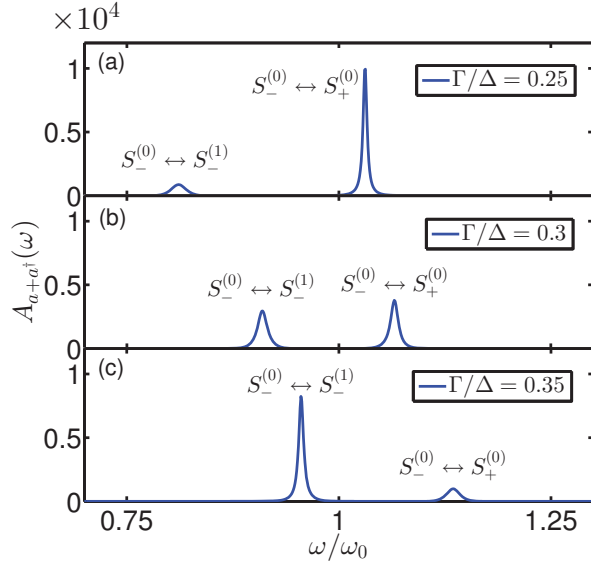


FIG. 5. (Color online) Spectral function  $A_{a+a^\dagger}(\omega)$  in different regimes. Each peak is associated with a given transition as indicated. The other parameters correspond to those in Fig. 2. We have used  $\alpha = 5 \times 10^{-4}$  in Eq. (13).

Notice that if the ground state of the electronic system is the doublet, the photons remain decoupled, and implicitly  $\Sigma_{\text{el}}$  vanishes. In this case, the transmission across the cavity is not affected by the electronic system. In this situation, no matter how close the avoided level crossing is to the QCP, there will always be just a single peak in the spectral density. Therefore, the discussion that follows refers mostly to the singlet side of the QCP. In our approach we have computed  $\Sigma_{\text{el}}(\omega)$  exactly, by evaluating  $\mathcal{F}^R(\omega)$  and a first approximation for  $\mathcal{D}^R(\omega)$  at the level of NRG, and by using a constant value for the photonic part.

In Fig. 5 we present the NRG results for  $A_{a+a^\dagger}(\omega)$ , when the system has a singlet ground state. When the system is off-resonance, there is always one peak in  $A_{a+a^\dagger}(\omega)$  formed at  $\omega \sim \omega_0$ , which corresponds to the transition from the ground state to the first photonic level with a width  $\kappa$  (panels (a) and (c) in Fig. 5). This peak is mainly determined by  $\mathcal{D}_0^R(\omega)$ , and gives the spectral density of the non-interacting cavity. The other peak, much smaller in amplitude and shifted away from  $\omega_0$ , is due to the electron-photon interaction. Its position is given by the energy of the singlet Shiba state within the gap and its height is proportional to the weight of the photonic transition amplitude between the ground and the excited state. In Fig. 5(b) we represent the situation when the system is at resonance:  $E_{S_+} \simeq \hbar\omega_0$ . Now, both transitions, corresponding to  $S_-^{(0)} \rightarrow S_-^{(1)}$  and  $S_-^{(0)} \rightarrow S_+^{(0)}$ , are similar in amplitude and considerably shifted to either side of  $\omega_0$ .

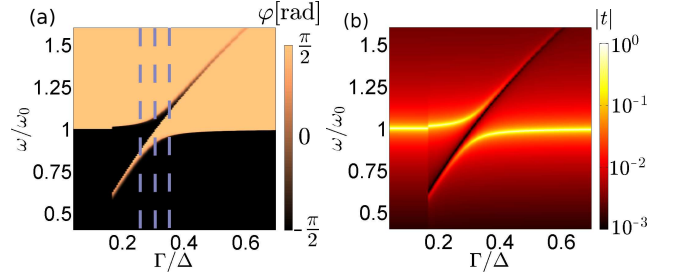


FIG. 6. (Color online) Density plots for the phase and absolute value of the transmission through the cavity. The three dashed lines correspond to the cuts along which the phase and amplitude of the transmission are displayed in Figs. 7 and 8.

## B. Transmission across the cavity

In our setup we consider that a microwave pulse comes from the left side and is either transmitted across the cavity to the right side, or reflected back. This can be viewed as a scattering problem and the response can be addressed in terms of the many body  $S$ -matrix  $\hat{S}$ . Energy conservation implies that the transition amplitude between some incoming  $|i\rangle$  and outgoing  $|f\rangle$  scattering states is related to the on-shell  $T$ -matrix through

$$\langle f|\hat{S}|i\rangle = \delta_{fi} + 2\pi i\delta(E_f - E_i)\langle f|\mathcal{T}|i\rangle, \quad (19)$$

where  $\langle f|\mathcal{T}|i\rangle$  is the on-shell  $T$ -matrix. By applying the path integral formalism (see Appendix C for details) we can relate the on-shell  $T$ -matrix to the Green's functions for the photons in the cavity

$$\begin{aligned} \text{Im}\mathcal{T}(\omega) &= \pi\lambda_{\mathbf{q}_f}\lambda_{\mathbf{q}_i}A_{a+a^\dagger}(\omega), \\ \text{Re}\mathcal{T}(\omega) &= \lambda_{\mathbf{q}_f}\lambda_{\mathbf{q}_i} \int d\omega' \frac{A_{a+a^\dagger}(\omega')}{\omega - \omega'}. \end{aligned} \quad (20)$$

If we further assume that the density of states  $\rho(\omega)$  for the modes in the external transmission lines varies slowly with the frequency around  $\omega = \omega_{\mathbf{q}}$ , and that the coupling  $\lambda_{\mathbf{q}}$  is approximately constant, we can write the transmission

$$t(\omega) = 2\pi i\rho(\omega)\mathcal{T}(\omega) = i\mathcal{J}(\omega)\mathcal{D}^R(\omega), \quad (21)$$

with  $\mathcal{D}^R(\omega)$  the Fourier transform of  $\mathcal{D}^R(t)$  defined in Eq. (14). We define the amplitude  $|t(\omega)|$  and the phase  $\varphi(\omega)$  of the transmission appearing in Eq. (21) through

$$t(\omega) = |t(\omega)|e^{i\varphi(\omega)}. \quad (22)$$

In Fig. 6 we display a density plot of these two quantities, while in Figs. 7 and 8 we display the same quantities along three cuts at fixed  $\Gamma/\Delta$  ratios.

It is straightforward to understand the amplitude behavior, since  $|t(\omega)|$  follows closely the behavior of the spectral function  $A_{a+a^\dagger}(\omega)$ , except for some small asymmetric contributions coming from the real part of the Green's function, which in the present calculations was

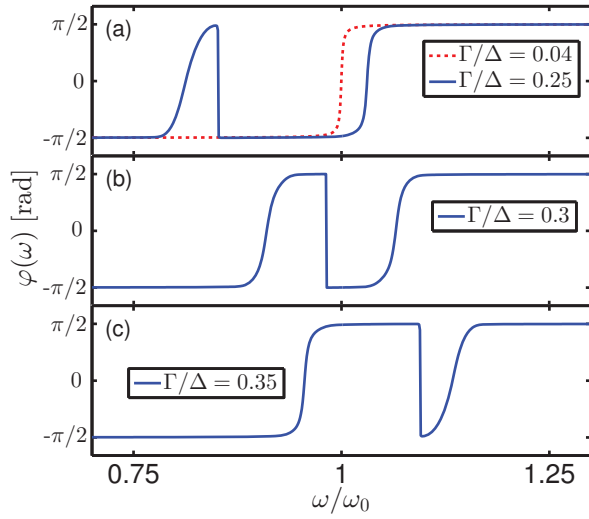


FIG. 7. (Color online) Phase of the transmission through the cavity when the system is in the singlet ground state, corresponding to  $x > x_{\text{QCP}}$ . The three panels correspond to the vertical cuts in Fig. 6 (a). For  $x < x_{\text{QCP}}$  the system simply shows a jump of  $\pi$  at  $\omega/\omega_0 = 1$  (displayed as a red dashed line in panel (a)).

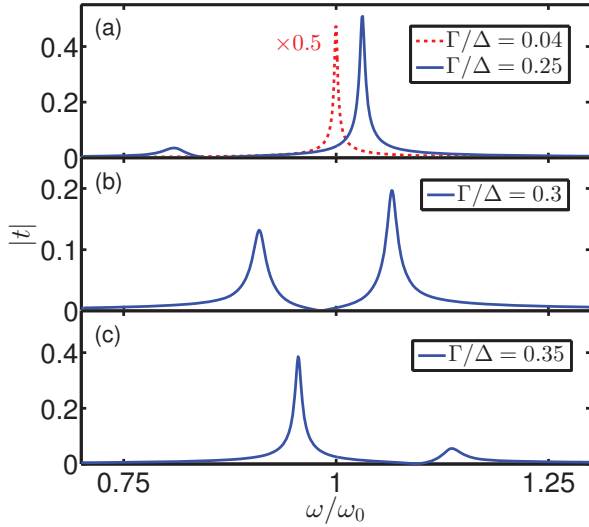


FIG. 8. (Color online) Absolute value for the amplitude of the transmission through the cavity for the same values of  $\Gamma/\Delta$  as in Fig. 7. The dashed red line in panel (a) represent the transmission amplitude when the system is in a doublet ground state, and corresponds to the otherwise free cavity.

computed by a Hilbert transform. The peaks in  $|t(\omega)|$  can be understood along the same lines as those for  $A_{a+a^\dagger}(\omega)$ , which we discussed in Sec. III A. The important point we want to make here is that the Shiba states leave a clear fingerprint in this measurable quantity. By tuning the system parameters, the coupling can be resonant, and the strength of the interaction can be measured experimentally [7]. If the avoided level crossing is tuned close to the QCP in the singlet region, then, by crossing through

the QCP into the doublet region (by tuning  $\Gamma$  for example), the photonic transition between the ground and the excited states becomes blocked, and the signal coming from these states must disappear. In the doublet region, the transmission is represented by the red dashed line in Fig. 8(a). This offers us a unique approach to exactly pinpoint the QPT.

The other quantity of interest that is accessible experimentally is the change in the phase of the transmission. In the absence of the electronic system,  $\varphi(\omega)$  shows a change of  $\pi$  radians as a function of the incoming microwave frequency  $\omega$  at the resonance frequency  $\omega = \omega_0$ . This is clearly visible in Fig. 6(a) when  $x < x_{\text{QCP}}$ , and the ground state is the doublet. In the doublet region, the phase will always present a single jump of  $\pi$  (indicated by the dashed line in Fig. 7(a)). In the singlet region close to the avoided level crossing, the coupling to the electronic system becomes important and the self-energy  $\Sigma_{\text{el}}$  increases. Furthermore, the light-matter interaction introduces more phase jumps of  $\pm\pi$  each time an excited Shiba state (within the singlet channel) is crossed. In contrast to the absolute value of the transmission amplitude, for which the signal can be weak, the phase change could give a much clearer signature of the presence of the Shiba states. For a true bound state with zero width, the phase will always show an abrupt jump of  $\pm\pi$ , the smooth steps visible in Fig. 7 being numerical artifacts due to the finite broadening of the bound states.

#### IV. CONCLUDING REMARKS

We have studied a hybrid system that consists of a quantum dot coupled to superconducting leads and also to a microwave cavity. In the absence of photons, such an electronic system develops multiple Shiba states inside the superconducting gap [20]. They have been recently investigated by using subgap spectroscopy [37]. The competition between them drives the system through a quantum phase transition. On one side of the transition, the ground state is a doublet, while on the other side it is a singlet.

It is accepted by now that coupling a mesoscopic device, such as a tunneling junction or a quantum dot, to a cavity, provides a non-invasive way to explore electronic processes [2, 5, 8]. Along this line, in the present work we demonstrate that coupling a mesoscopic system, that supports Shiba states, to a microwave cavity, offers a controllable way to monitor these localized states [7] and their evolution across the quantum phase transition. If the ground state is a doublet, the cavity is insensitive to the presence of the electronic system, and the transmission is unaltered. If the system is tuned across the quantum critical point in the region where the ground state is a singlet, the coupling between the electronic system and the cavity leaves distinctive features in the transmitted signal. The computational methodology was based on the numerical renormalization group approach supple-

mented by analytical calculations.

### ACKNOWLEDGMENTS

We are thankful to Gergely Zarand, Andras Palyi and Vidar Gudmundsson for insightful comments and lively discussions. This work was supported by the Romanian National Authority for Scientific Research and Innovation, UEFISCDI, project number PN-II-RU-TE-2014-4-0432, and by the Hungarian research fund OTKA under grant No. K105149.

### Appendix A: Numerical renormalization group approach

We solve the Hamiltonian in Eq. (6) by using the numerical renormalization group. We shall discuss the situation with the left-right symmetry and  $\varphi_\alpha = 0$ , with  $\alpha = \{L, R\}$  (no phase difference between the superconducting gaps on the left/right leads). We first perform a unitary transformation [30] and introduce a new basis

$$\begin{pmatrix} c_{e\mathbf{k}\sigma} \\ c_{o\mathbf{k}\sigma} \end{pmatrix} = \frac{1}{\sqrt{2}} \begin{pmatrix} 1 & 1 \\ -1 & 1 \end{pmatrix} \begin{pmatrix} c_{L\mathbf{k}\sigma} \\ c_{R\mathbf{k}\sigma} \end{pmatrix}.$$

The advantage of this even-odd basis over the left-right one is that the odd channel becomes decoupled and the 'impurity' remains coupled only to the even channel. Performing a logarithmic discretization of the conduction band by using a parameter  $\Lambda > 1$ , followed by a tridiagonalization procedure that maps the problem on the Wilson chain [23], the leads Hamiltonian transforms to

$$H_{\text{leads}} = \sum_{n=0}^{\infty} \sum_{\sigma} \left( t_n f_{n\sigma}^\dagger f_{n+1\sigma} + \Delta f_{n\uparrow}^\dagger f_{n\downarrow}^\dagger + \text{H.c.} \right),$$

where  $t_n$  is the hopping between nearest neighbor sites along the Wilson chain, which decreases exponentially fast,  $t_n \sim \Lambda^{-n/2}$ , and  $f_{n\sigma}^\dagger$  is the fermionic creation operator at the  $n$ -th site. The 'impurity' is coupled to the first site of the Wilson chain, by the tunneling Hamiltonian

$$H_{\text{tun}} = \sum_{\sigma} \left( \sqrt{2}V f_{0\sigma}^\dagger d_{\sigma} + \text{H.c.} \right). \quad (\text{A1})$$

The 'impurity' is a complex object that takes into account all the bosonic states for the photons. In our calculation we have considered only five such photonic states. Increasing this number does not visibly affect our results. The Hamiltonian for the 'impurity'

$$H_{\text{impurity}} = H_{\text{dot}} + H_{\text{cav}} + H_{\text{int}} \quad (\text{A2})$$

remains unaffected by the unitary transformation, and is the sum of Hamiltonian terms discussed in Sec. II A and given in Eqs. (1), (3) and (4). The model is SU(2) invariant, as the total Hamiltonian commutes with the spin operator, which allows us to keep track of this symmetry when indexing the eigenstates of the Hamiltonian.

### Appendix B: Photon Spectral Function

In this appendix we shall give a brief derivation of Dyson Eq. (17). The goal is to compute the bosonic Green's function from eq. (14) accurately. We start by defining the retarded Green's function of two bosonic operators  $\mathcal{O}_1$  and  $\mathcal{O}_2$  as

$$\mathcal{D}_{\mathcal{O}_1, \mathcal{O}_2}^R(t) = -i\theta(t) \langle [\mathcal{O}_1(t), \mathcal{O}_2(0)] \rangle. \quad (\text{B1})$$

Its Fourier transform,  $\mathcal{D}_{\mathcal{O}_1, \mathcal{O}_2}^R(\omega)$ , satisfies the equation of motion

$$\omega \mathcal{D}_{\mathcal{O}_1, \mathcal{O}_2}^R(\omega) = \langle [\mathcal{O}_1, \mathcal{O}_2] \rangle - \mathcal{D}_{\mathcal{O}_1, [\mathcal{O}_2, H]}^R(\omega). \quad (\text{B2})$$

Applying this formula successively, first for  $\mathcal{O}_1 = a + a^\dagger$ ,  $\mathcal{O}_2 = a + a^\dagger$ , and then for  $\mathcal{O}_1 = a^\dagger - a$ ,  $\mathcal{O}_2 = a + a^\dagger$ , we immediately obtain eq. (17) [26]. Notice that the superconducting gap does not enter explicitly in Eq. (17). The correlator  $\mathcal{F}^R(\omega)$  is computed directly from the NRG.

### Appendix C: T-matrix for the external photon bath

In this appendix we derive the expression for the  $T$ -matrix for the external photon bath. It is most convenient to work with a path integral formalism. Our goal is to express the full Green's function for the bosonic modes of the photons in the external transmission lines. In this approach, the electronic part plays no role, and can be integrated out from the beginning. The partition and the generating functions can be constructed by replacing the bosonic fields by time dependent complex variables [38]:  $\{b_{\beta q}, b_{\beta q}^\dagger, a, a^\dagger\} \rightarrow \{b_{\beta q}, \bar{b}_{\beta q}, a, \bar{a}\}$ . For the generating function it follows:

$$\mathcal{Z}[\eta, \bar{\eta}] = \int D[b, \bar{b}] D[a, \bar{a}] e^{-i\mathcal{S}[b, \bar{b}, a, \bar{a}] + i\bar{\eta} \cdot b + i\bar{b} \cdot \eta}, \quad (\text{C1})$$

with the total action consisting of several terms:  $\mathcal{S} = \mathcal{S}_{\text{bath}} + \mathcal{S}_{\text{cav}} + \mathcal{S}_{\text{int}}$ . Here we have used the notation:  $\bar{\eta} \cdot b = \sum_{\beta, q} \int dt \bar{\eta}_{\beta q}(t) b_{\beta q}(t)$ . The non-interacting part  $\mathcal{S}_{\text{bath}}$  describes the photons in the external bath and is given by

$$\mathcal{S}_{\text{bath}} = - \sum_{\beta=\{L, R\}} \sum_q \int dt dt' \bar{b}_{\beta q}(t) \mathcal{D}_{0, \beta q}^{-1}(t - t') b_{\beta q}(t'),$$

with  $\mathcal{D}_{0, \beta q}(t - t')$  the corresponding non-interacting Green's function. The cavity is described by the action

$$\mathcal{S}_{\text{cav}} = - \int dt dt' \bar{a}(t) \mathcal{D}^{-1}(t - t') a(t').$$

Here  $\mathcal{D}(t - t')$  is the Green's function for the photons in the cavity, that contains the self-energy contribution by integrating the electronic part. The interaction part describes the hybridization of the modes in the bath with those in the cavity

$$\mathcal{S}_{\text{int}} = \sum_{\beta=\{L, R\}} \sum_q \lambda_q \int dt [\bar{a}(t) b_{\beta q}(t) + \text{c.c.}].$$



The full Green's function for the external modes can be written as a functional differentiation

$$\mathcal{D}_{\beta q, \beta' q'} = -i \frac{\delta^2 \ln \mathcal{Z}[\eta, \bar{\eta}]}{\delta \bar{\eta}_{\beta q}(t) \delta \eta_{\beta' q'}(t')} \Big|_{\eta, \bar{\eta} \rightarrow 0}. \quad (\text{C2})$$

Then the expression for the  $T$ -matrix can be obtained by shifting the integration argument in the exponent of the

generating function in (C1)

$$b_{\beta q} \rightarrow b_{\beta q} - \int dt' \mathcal{D}_{0, \beta q}(t - t') \eta_{\beta q}(t'),$$

followed by the differentiation (C2). Finally, the full Green's function is:

$$\begin{aligned} \mathcal{D}_{\beta q_f, \beta' q_i}(t - t') &= \delta_{\beta \beta'} \delta_{q_f q_i} \mathcal{D}_{0, \beta q_i}(t - t') - \\ &- i \lambda_{q_f} \lambda_{q_i} \int dt_1 dt'_1 \mathcal{D}_{0, \beta q_f}(t - t_1) \mathcal{D}(t_1 - t'_1) \mathcal{D}_{0, \beta' q_i}(t'_1 - t'), \end{aligned}$$

which allows us to identify the expression for the  $T$ -matrix, given in Eq. (20).

- 
- [1] Z.-L. Xiang, S. Ashhab, J. Q. You, and F. Nori, *Rev. Mod. Phys.* **85**, 623 (2013).
  - [2] A. Wallraff, D. I. Schuster, A. Blais, L. Frunzio, R. S. Huang, J. Majer, S. Kumar, S. M. Girvin, and R. J. Schoelkopf, *Nature* **431**, 162 (2004).
  - [3] T. Frey, P. J. Leek, M. Beck, K. Ensslin, A. Wallraff, and T. Ihn, *Appl. Phys. Lett.* **98**, 262105 (2011).
  - [4] A. Rundquist, A. Majumdar, and J. Vuckovic, *Applied Physics Letters* **99** (2011).
  - [5] M. R. Delbecq, V. Schmitt, F. D. Parmentier, N. Roch, J. J. Vienne, G. Fève, B. Huard, C. Mora, A. Cottet, and T. Kontos, *Phys. Rev. Lett.* **107**, 256804 (2011).
  - [6] G.-W. Deng, D. W. Henriët, S.-X. Li, H.-O. Li, G. Cao, M. Xiao, G.-C. Guo, M. Schiro, K. Le Hur, and G.-P. Guo, *arXiv:1509.06141v2* (2015).
  - [7] C. Janvier, L. Tosi, L. Bretheau, C. O. Girit, M. Stern, P. Bertet, P. Joyez, D. Vion, D. Esteve, M. F. Goffman, H. Pothier, and C. Urbina, *Science* **349**, 1199 (2015).
  - [8] T. Frey, P. J. Leek, M. Beck, A. Blais, T. Ihn, K. Ensslin, and A. Wallraff, *Phys. Rev. Lett.* **108**, 046807 (2012).
  - [9] A. F. van Loo, A. Fedorov, K. Lalumière, B. C. Sanders, A. Blais, and A. Wallraff, *Science* **342**, 1494 (2013).
  - [10] M. Kulkarni, O. Cotlet, and H. E. Türeci, *Phys. Rev. B* **90**, 125402 (2014).
  - [11] A. Blais, R.-S. Huang, A. Wallraff, S. M. Girvin, and R. J. Schoelkopf, *Phys. Rev. A* **69**, 062320 (2004).
  - [12] A. Cottet, T. Kontos, and B. Douçot, *Phys. Rev. B* **91**, 205417 (2015).
  - [13] J. Sköglberg, T. Löfwander, V. S. Shumeiko, and M. Fogelström, *Phys. Rev. Lett.* **101**, 087002 (2008).
  - [14] O. Dmytruk, M. Trif, and P. Simon, *Phys. Rev. B* **92**, 245432 (2015).
  - [15] K. Le Hur, *Phys. Rev. B* **85**, 140506 (2012).
  - [16] O. Dmytruk, M. Trif, C. Mora, and P. Simon, *arXiv:1510.03748v2* (2015).
  - [17] M. Schiró and K. Le Hur, *Phys. Rev. B* **89**, 195127 (2014).
  - [18] V. Gudmundsson, O. Jonasson, C.-S. Tang, H.-S. Goan, and A. Manolescu, *Phys. Rev. B* **85**, 075306 (2012).
  - [19] T. Arnold, C.-S. Tang, A. Manolescu, and V. Gudmundsson, *Phys. Rev. B* **87**, 035314 (2013).
  - [20] H. Shiba, *Progress of theoretical Physics* **40**, 435 (1968).
  - [21] N. Y. Yao, C. P. Moca, I. Weymann, J. D. Sau, M. D. Lukin, E. A. Demler, and G. Zaránd, *Phys. Rev. B* **90**, 241108 (2014).
  - [22] U. C. Mendes and C. Mora, *New Journal of Physics* **17**, 113014 (2015).
  - [23] K. G. Wilson, *Rev. Mod. Phys.* **47**, 773 (1975).
  - [24] H. R. Krishna-murthy, J. W. Wilkins, and K. G. Wilson, *Phys. Rev. B* **21**, 1003 (1980).
  - [25] A. C. Hewson and D. Meyer, *Journal of Physics: Condensed Matter* **14**, 427 (2002).
  - [26] G. S. Jeon, T.-H. Park, and H.-Y. Choi, *Phys. Rev. B* **68**, 045106 (2003).
  - [27] A. C. Hewson, *The Kondo Problem to Heavy Fermions* (Cambridge University Press, Cambridge, 1993).
  - [28] A. V. Rozhkov and D. P. Arovass, *Phys. Rev. Lett.* **82**, 2788 (1999).
  - [29] M. Zonda, V. Pokorný, V. Janis, and T. Novotný, *Scientific Reports* **5**, 8821 (2015).
  - [30] T. Hecht, A. Weichselbaum, J. von Delft, and R. Bulla, *Journal of Physics: Condensed Matter* **20**, 275213 (2008).
  - [31] T. Meng, S. Florens, and P. Simon, *Phys. Rev. B* **79**, 224521 (2009).
  - [32] E. Jaynes and F. Cummings, *Proceedings of the IEEE* **51**, 89 (1963).
  - [33] Leonard Mandel, Emil Wolf *Optical Coherence and Quantum Optics* (Cambridge University Press, 1995).
  - [34] G.-W. Deng, D. Wei, J. R. Johansson, M.-L. Zhang, S.-X. Li, H.-O. Li, G. Cao, M. Xiao, T. Tu, G.-C. Guo, H.-W. Jiang, F. Nori, and G.-P. Guo, *Phys. Rev. Lett.* **115**, 126804 (2015).
  - [35] G. Gasse, C. Lupien, and B. Reulet, *Phys. Rev. Lett.* **111**, 136601 (2013).
  - [36] R. Bulla, A. C. Hewson, and T. Pruschke, *Journal of Physics: Condensed Matter* **10**, 8365 (1998).
  - [37] M. Gaass, S. Pfaller, T. Geiger, A. Donarini, M. Grifoni, A. K. Hüttel, and C. Strunk, *Phys. Rev. B* **89**, 241405 (2014).
  - [38] John W. Negele, *Quantum Many-particle Systems* (Westview Press, 1998).